CrossMark

Progression of chromosomal damage induced by etoposide in G2 phase in a DNA-PKcs-deficient context

Micaela Palmitelli · Marcelo de Campos-Nebel · Marcela González-Cid

Abstract Etoposide (ETO), a drug used for the treatment of human tumors, is associated with the development of secondary malignancies. Recently, therapeutic strategies have incorporated chemosensitizing agents to improve the tumoral response to this drug. ETO creates DNA double-strand breaks (DSB) via inhibition of DNA topoisomerase II (Top2). To repair DSB, homologous recombination (HR) and non-homologous end-joining (NHEJ), involving D-NHEJ (dependent of the catalytic subunit of DNA-dependent protein kinase, DNA-PKcs) and B-NHEJ (backup repair pathway) are activated. We evaluated the progression of the DNA damage induced by the Top2 poison ETO in G2 phase of human HeLa cells after chemical inhibition of DNA-PKcs with NU7026. Compared to ETO treatment alone, this combined treatment resulted in a twofold higher rate of chromatid breaks and exchanges when analysis was performed in the following metaphase. Moreover, when analysis was performed in the second metaphase following treatment, increases in the percentage of micronuclei with H2AX (biomarker for DSB) foci in binucleated cells and dicentric chromosomes were seen. In postmitotic G1 phase, a close association between unresolved DSB and meiotic recombination 11 homolog A (MRE11) signals was observed, demonstrating the contribution of MRE11 in the DSB repair by B-NHEJ. Hence, chemical inhibition of DNA-PKcs impaired both D-NHEJ and HR repair pathways, altering the maintenance of chromosomal integrity and cell proliferation. Our results suggest that the chemosensitizing effectiveness of the DNA-PKcs inhibitor and the survival rate of aberrant cells may contribute to the development of therapy-related tumors.

Keywords Topoisomerase II poison · DNA damage · DSB repair pathway · G2 phase · DNA-PKcs chemical inhibition

Abbreviations

A-NHEJ	Alternative non-homologous end-joining
ATM	Ataxia-telangiectasia mutated
B-NHEJ	Backup non-homologous end-joining
BN	Binucleated cells
BrdU	5-Bromo-2′-deoxyuridine
C-NHEJ	Classic non-homologous end-joining
CENP-F	Centromere protein F
D-NHEJ	DNA-PKcs-dependent non-homologous end-joining
DAPI	4,6-Diamidino-2-phenylindole
DMSO	Dimethyl sulfoxide
DNA-PKcs	DNA-dependent protein kinase catalytic subunit

Responsible Editor: Dean A. Jackson

M. Palmitelli · M. de Campos-Nebel · M. González-Cid (✉)
Laboratorio de Mutagénesis, Instituto de Medicina Experimental, IMEX-CONICET, Academia Nacional de Medicina, J. A. Pacheco de Melo 3081, 1425 Buenos Aires, Argentina
e-mail: margoncid@hematologia.anm.edu.ar

Springer

DSB	Double-strand breaks
ETO	Etoposide
FISH	Fluorescent in situ hybridization
FITC	Fluorescein isothiocyanate
γH2AX	Histone H2AX-phosphorylated on serine 139
HR	Homologous recombination
MI	Mitotic index
MN	Micronuclei
MRE11	Meiotic recombination 11 homolog A
NU7026	2-(Morpholin-4-yl)-benzo[h]chromen-4-one
PBS	Phosphate-buffered saline
PFA	Paraformaldehyde
PI	Propidium iodide
Rad51	DNA repair protein RAD51 homolog 1
SCE	Sister chromatid exchanges
Top2	Topoisomerase II

Introduction

Etoposide (ETO), a semisynthetic derivative of podophyllotoxin, is one of the most widely used drugs for the treatment of various types of human malignancies, including leukemia, lymphoma, and solid tumors (Tammaro et al. 2013). ETO creates DNA double-strand breaks (DSB) via inhibition of DNA topoisomerase II (Top2). This enzyme solves topological problems of DNA during replication, transcription, chromosome condensation, and segregation (Nitiss 2009). The reaction catalyzed by Top2 consists of the interaction of the homodimeric enzyme with DNA; each subunit cleaves one strand of the double helix, and this leads to the formation of a transient DSB (Montecucco and Biamonti 2007). Top2 poisons such as ETO specifically inhibit the religation step and thereby lock covalently linked Top2 to DNA leading to permanent DSB formation (Deweese and Osheroff 2009). In human cells, these lesions are repaired using two mechanistically and genetically different pathways: homologous recombination (HR) and non-homologous end-joining (NHEJ) (de Campos-Nebel et al. 2010). HR is a high-fidelity repair mechanism that occurs preferentially during the late S/G2 phases of the cell cycle when the replicated (genetically identical) sister chromatids are present. In contrast, NHEJ functions independently of sister chromatids and occurs in all phases of the cell

cycle (Dueva and Iliakis 2013). This process simply pieces together the broken DNA ends irrespective of their origin, resulting in an error-prone pathway, with frequent loss or addition of a few nucleotides at the break site.

Under normal conditions, cells of higher eukaryotes employ preferentially this classic NHEJ (C-NHEJ) pathway to quickly remove DSB from the genome. However, cells deficient in C-NHEJ are able to rejoin the majority of DSB by utilizing an alternative NHEJ (A-NHEJ) pathway, which is more error-prone than C-NHEJ. Although A-NHEJ is more evident in these cells, it is also detectable in wild-type cells when an excessive number of DSB is present. This mechanism is likely to be an evolutionarily older pathway with a less efficient synapsis process that rejoins DNA ends with slow kinetics (Lieber 2010). Furthermore, A-NHEJ appears to be responsible for chromosomal translocations found in cancer cells (Boboila et al. 2012) and thus makes a major contribution to DSB repair in these cells (Sallmyr et al. 2008).

The catalytic subunit of DNA-dependent protein kinase (DNA-PKcs) is the key component of C-NHEJ that controls and drives the DSB repair in cells of higher eukaryotes (Mladenov et al. 2013). For this reason, this pathway has also been termed DNA-PKcs-dependent non-homologous end-joining (D-NHEJ); we adopted this expression here. Since A-NHEJ gains functional importance when D-NHEJ mechanism fails, it is considered to be a backup repair process and has been abbreviated as backup non-homologous end-joining (B-NHEJ) (Mladenov and Iliakis 2011). The role of DNA-PKcs in normal tissues is to promote DSB repair and chromosomal stability, preserving the integrity of the genome. Altered activity of DNA-PKcs facilitates accumulation of mutations and genome instability, both known precursors of carcinogenic transformation (Hsu et al. 2012).

Most anticancer therapies generate multiple DSB to eliminate actively proliferating tumor cells but damaging simultaneously non-tumor cells which can develop structural chromosome rearrangements and might be a source of new therapy-related tumors in treated patients (Leone et al. 2010). In this regard, previous studies have shown that ETO is associated with the severe side effect of secondary malignancies resulting from drug-induced chromosome translocations (Cowell and Austin 2012; Pendleton et al. 2014). Therefore, a better understanding of how cells repair ETO-induced DSB is required to

improve the therapeutic efficacy and diminish the adverse side effects of this drug.

Several papers demonstrated a strong effect of ETO on survival and chromosome damage (Darroudi and Natarajan 1989; Jeggo et al. 1989; Jin et al. 1998; Katsube et al. 2011) in D-NHEJ-deficient mammalian cell lines. Moreover, our previous results have shown that D-NHEJ allows Chinese hamster cells that were treated with Top2 poisons during S/G2 to progress into the following interphase (Elguero et al. 2012). Here, we evaluated the role of potentially error-prone D-NHEJ and B-NHEJ repair pathways in the conversion of persistent DNA damage to chromosomal rearrangements following ETO treatment in G2 phase, since these pathways may be associated with cancer development. We focused on G2 damaged cells because this is a critical stage of the cell cycle where both the expression and the activity of the α isoform of Top2 are increased, and D-NHEJ as well as HR repair pathways can potentially repair ETO-induced lesions. Moreover, Wu et al. (2008) reported that B-NHEJ activity was markedly increased in the G2 phase in cells deficient in D-NHEJ.

In the present investigation, we show that chemical inhibition of DNA-PKcs impaired both D-NHEJ and HR repair pathways in the immediate metaphase after ETO treatment in human HeLa cells. Furthermore, in post-mitotic G1 phase surviving cells, we observed an increased frequency of micronuclei and unresolved DSB, which showed a close association with meiotic recombination 11 homolog A (MRE11) signals, consistent with a role for MRE11 in DSB repair by B-NHEJ. In the second metaphase following ETO treatment with DNA-PKcs chemically inhibited, an increase in dicentric chromosomes was observed. Both micronuclei and dicentric chromosomes are precursors of genomic instability that can potentially result in the development of secondary neoplasms after Top2 poison treatments.

Materials and methods

Chemicals

ETO (Chemical Abstracts Service Registry Number (CAS no.) 33419-42-0, Sigma-Aldrich), 2-(morpholin-4-yl)-benzo[h]chromen-4-one (NU7026) (CAS no. 154447-35-5, Calbiochem), and cytochalasin B (CAS no. 14930-96-2, Calbiochem) were dissolved in dimethyl sulfoxide (DMSO) (CAS

no. 67-68-5, Mallinckrodt Baker). Thymidine (CAS no. 50-89-5, Sigma-Aldrich), aphidicolin (CAS no. 38966-21-1, Calbiochem), and 5-bromo-2′-deoxyuridine (BrdU, CAS no. 59-14-3, Sigma-Aldrich) were dissolved in bidistilled water.

Cell cultures and drug treatments

Human cervical carcinoma HeLa cells (modal number=66±3 chromosomes per cell) were grown in complete medium containing RPMI 1640 (Gibco) supplemented with 10 % fetal bovine serum (Natocor), 2 mM L-glutamine (Gibco), 100 units/ml penicillin, and 100 μg/ml streptomycin. Cultures were maintained at 37 °C in a humidified atmosphere of 5 % CO_2 in air. Cells were pre-treated with or without NU7026 10 μM for 1 h, co-incubated with ETO 2 μg/ml for 1 h, and kept in medium containing NU7026 for different time points according to the assay. Control cultures were exposed to equivalent volumes of corresponding solvents of the drugs and grown under identical conditions.

Cell synchronization and γH2AX detection

A thymidine-aphidicolin sequential double block was used to synchronize the cells at the G1/S border. Eight hours after release, the percentage of cells in G2/M phase was checked by flow cytometry with propidium iodide (PI) and was 66.2±3.3 % (% of cells at G2/M in asynchronous cultures was 17.7±7.5). G2 phase synchronized HeLa cell line was grown on coverslips in 35-mm dishes and exposed to ETO 2 μg/ml for 1 h and DMSO 0.5 % for 2 h or mock treated. After washing twice in phosphate-buffered saline (PBS), cells were fixed with 2 % paraformaldehyde (PFA) and permeabilized with 0.25 % Triton X-100 in PBS for 20 min at room temperature. Immunofluorescence was performed using primary antibodies against centromere protein F (CENP-F) (1:100; Santa Cruz Biotechnology) and histone H2AX-phosphorylated on serine 139 (γH2AX) (1:100; Cell Signaling), followed by exposure to fluorescein isothiocyanate (FITC)- or Texas Red-labeled secondary antibodies (1:200), respectively. DNA was stained with 4,6-diamidino-2-phenylindole (DAPI, Vector Laboratories) containing antifade solution. The γH2AX foci number per nucleus

was analyzed by visual scoring in 100 CENP-F-positive nuclei.

Structural chromosome alterations and mitotic index

Exponentially growing HeLa cells were treated with NU7026, ETO, or a combination of both drugs as previously described and incubated for 5–6 h to reach the immediate metaphase. Colcemid 0.1 μg/ml was added 90 min before harvesting; cells were exposed to hypotonic solution KCl 0.075 M, fixed in 3 methanol/1 acetic acid, and stained with 10 % Giemsa for 2.5 min. For each treatment, 100 metaphases were analyzed for the induction of chromatid breaks and exchanges. Complete and incomplete chromatid exchanges in the same configuration were considered as complex exchanges. The gaps were excluded from the analysis of chromosome aberration frequencies. Mitotic index (MI) was calculated as the number of metaphases among 2,000 nuclei and expressed as a percentage.

Rad51 immunofluorescence and sister chromatid exchanges (SCE)

For the evaluation of HR, the following methodologies were used:

1. HeLa cells were grown on coverslips, treated, and incubated for 5–6 h. Cells were then fixed with 2 % PFA and permeabilized with 0.25 % Triton X-100 in PBS. Immunofluorescence was performed using primary antibody against DNA repair protein RAD51 homolog 1 (Rad51) (1:250; Santa Cruz Biotechnology) followed by exposure to Texas Red-conjugated secondary antibody (1:200), and DNA was stained with DAPI. The number of Rad51 foci per nucleus was analyzed by visual scoring in 100 cells.
2. HeLa cells were incubated in the presence of 10 μg/ml BrdU for 44 h (about two rounds of replication). Then, cells were treated and incubated for 5–6 h. Colcemid was added 90 min before harvesting, and cells were exposed to hypotonic solution and fixed. Air-dried chromosome preparations were made and a modification of the fluorescence-plus-Giemsa method was applied to obtain harlequin chromosomes. The average frequency of SCE per chromosome was determined from the analysis of 25 metaphases.

Micronucleus formation in binucleated cells

Exponentially growing HeLa cell line was seeded on coverslips, treated, and incubated for 10 h to reach the following cell cycle. Cytochalasin B 3 μg/ml was added during the last 4 h before harvesting, and cells were exposed to hypotonic solution for 8 min and fixed with 2 % PFA and permeabilized with 0.25 % Triton X-100. Indirect immunofluorescence was carried out using the primary antibody against γH2AX as described previously and DNA was stained with DAPI. The occurrence of γH2AX foci in the micronuclei (MN) and in the main nucleus was evaluated in at least 500 binucleated (BN) cells. The percentage of BN cells was scored in 1,000 cells for each treatment.

γH2AX and MRE11 co-localization analysis

Ten hours after ETO and NU7026-ETO treatments, BN cells were simultaneously labeled for γH2AX and MRE11 proteins, using a two-color immunofluorescence staining technique. Cells were permeabilized with 0.5 % Triton X-100 in PBS for 2.5 min and then fixed with 2 % PFA. To detect MRE11 foci, a primary antibody against MRE11 (1:500, Abcam) was used. Texas Red-conjugated and Alexa Fluor 488-conjugated (1:300) secondary antibodies were used for the detection of MRE11 and γH2AX, respectively. Measurements of co-localization of both proteins and the scoring of fluorescent nuclear foci were performed using confocal microscopy. BN cells with γH2AX foci were chosen for the analysis. Images were acquired using a FluoView FV1000 confocal microscope (Olympus) equipped with a Plan Apo 60X/1.42NA objective lens and processed using FV10-ASW software (Olympus) or ImageJ (NIH) Software packages. Z-stack images covering the whole nuclear volume, approximately 33 serial optical sections spaced by 0.3 μm, were captured. The fractions of co-localizing pixels in each component of a dual-color image were analyzed by means of M1 and M2 coefficients (Manders et al. 1993). Also, a correlation between both fluorophores was evaluated using the Pearson's correlation coefficient. A total of 20 BN-treated cells was examined.

G2/M checkpoint assay

HeLa cell cultures were treated and incubated for 28 h, then colcemid was added 90 min prior to harvest. Cells

were then fixed with 2 % PFA and permeabilized with 100 % methanol. Cells were immunostained with anti-phospho Ser10 histone H3 (1:50 Santa Cruz) antibody followed by Alexa Fluor 488-conjugated secondary antibody (1:250). RNAse A treatment and PI counterstaining were performed, and 30,000 cells were analyzed by flow cytometry (Becton Dickinson) to determine the cells in mitosis.

Whole chromosome painting using fluorescence in situ hybridization (FISH)

Exponentially growing HeLa cells were treated and incubated for 28 h adding BrdU during the last 8 h to detect the second mitosis. Metaphase chromosomes were obtained as described above, and FISH analysis was performed using painting probes for chromosomes 1, 2, and 4 labeled with Texas Red (Lexel, Argentina) according to the manufacturer's protocol. Subsequently, slides were incubated in blocking solution containing primary antibodies against BrdU (1:100; Santa Cruz Biotechnology) for 1 h, followed by exposure to secondary antibodies conjugated to Dye Light 488 (1:300), and DNA was stained with DAPI. The presence of translocation involving chromosomes 1, 2, and 4 per metaphase was scored in 20 BrdU-positive cells. The frequency of dicentric chromosome was evaluated in 50 cells on the same slides.

Results

ETO induces DNA DSB in G2 phase

HeLa cells enriched in G2 phase of the cell cycle were treated with DMSO or the Top2 poison ETO. γH2AX detection was scored in CENP-F-stained nuclei. CENP-F is a protein of the nuclear matrix that gradually accumulates during the cell cycle until it reaches peak levels in G2 and M phase cells, showing a strong pan-nuclear CENP-F staining in G2 phase cells (Liao et al. 1995; Kao et al. 2001). The 91.0 %±1.4 (mean±SD) of the untreated control cells and 87.0 % of the cells treated with DMSO presented ≤20 γH2AX foci per nucleus. On the other hand, 80.0±8.5 % of the cells treated with ETO showed >60 γH2AX foci per nucleus (Fig. 1). Additionally, in non-synchronized cells, similar numbers of γH2AX foci were observed in CENP-F-stained

nuclei when compared with cells enriched in G2 phase (Supplementary Fig. S1).

Together, our results show that treatment with ETO in G2 stage induces discrete γH2AX foci, which correlate with the generation of DSB.

D-NHEJ inhibition causes increased chromosome aberrations in ETO-treated cells

To determine the involvement of D-NHEJ in the repair of Top2-induced DSB, we evaluated the induction of chromosome aberrations following ETO treatment in the presence of the DNA-PKcs inhibitor NU7026 (Table 1). Conventional chromosome analysis at the first metaphase revealed that ETO treatment induced high levels of abnormal cells, as evidenced by an increase of chromatid-type aberrations, breaks, and exchanges, relative to levels in DMSO-treated cells. Untreated control and DMSO- or NU7026-treated cells were characterized by a low frequency of chromatid breaks. In the case of NU7026, an increased frequency of chromatid breaks, although not statistically significant, was observed. The exposure of HeLa cells to the combination of NU7026 and ETO yields a twofold higher rate of chromatid breaks (Fig. 2a) and exchanges (Fig. 2b) compared to ETO-treated cultures. In addition, we noted an associated reduction in MI, which affects the scoring of chromosome aberrations. NU7026-ETO significantly decreased the MI by ~85 % with respect to ETO alone (Fig. 2c). Furthermore, flow cytometry analysis confirmed an increase in the fraction of cells in G2/M phase following NU7026-ETO treatment in comparison with ETO (Supplementary Fig. S2). Regarding this, a clonogenic survival assay showed a hypersensitivity of HeLa cells treated with increasing doses of ETO in the presence of NU7026 (Supplementary Fig. S3). These results suggest that chemical inhibition of DNA-PKcs increases the frequency of cells with abnormal chromosome and decreases their viability, consistent with the role of D-NHEJ in the maintenance of genome integrity.

DNA-PKcs regulates the HR repair of ETO-induced DNA DSB

It has been previously reported that impairing D-NHEJ might result in channeling of DNA DSB repair towards HR. To investigate the role of the DNA-PKcs inhibition on HR regulation, we measured Rad51 foci formation (Fig. 2d). Rad51, a key protein in the HR repair of DSB,
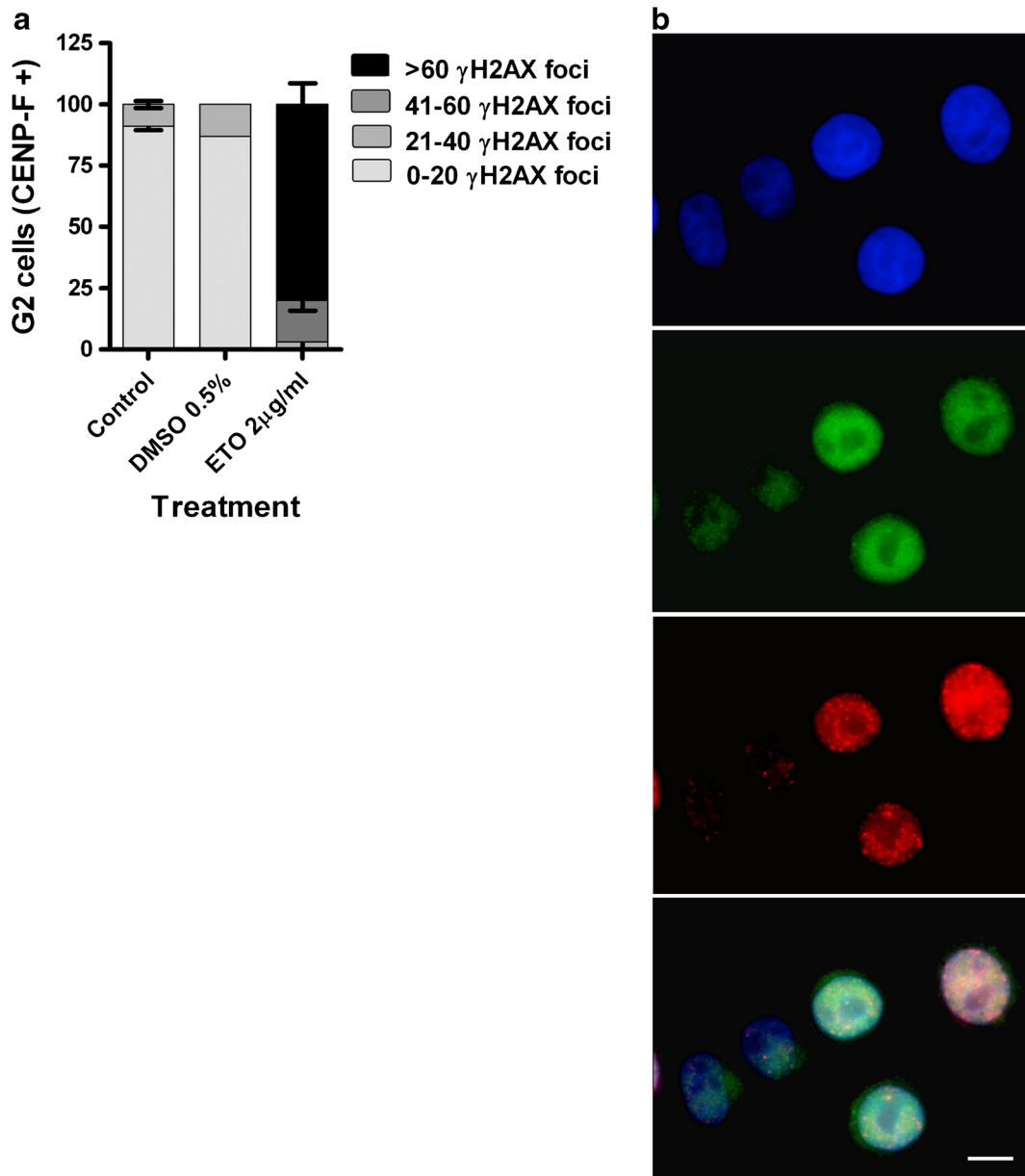
Fig. 1 DNA DSB induced by ETO in G2 synchronized HeLa human cells. **a** HeLa cells were treated with DMSO or ETO, and γH2AX foci number per nucleus was scored in G2 cells. *Error bars* represent the SD of two independent experiments. **b** Representative images of HeLa nuclei treated with ETO for 1 h. CENP-F (FITC) immunostaining was used to distinguish G2 cells, and γH2AX (Texas Red) immunostaining served as DSB marker. DNA was stained with DAPI. *Scale bar*, 10 μm

forms a nucleoprotein filament on the DNA that promotes strand invasion, a critical early step during mitotic recombination. At 5–6 h post-treatment with NU7026-ETO, cells exhibited a slight but significant increase in the number of Rad51 foci per nuclei (9.1±6.6) compared to ETO-treated cells (6.9±5.7), consistent with a major use of HR to repair Top2-induced DSB when

DNA-PKcs is chemically inhibited. In addition, using the induction of SCE per chromosome as an alternative endpoint of HR activity (Fig. 2e) showed that a fraction of the ETO-induced DSB that undergo repair by HR gives rise to SCE (0.18±0.05 vs. 0.12±0.05 in DMSO-treated cells, $p=0.0001$). In comparison, the combination of NU7026-ETO produced a frequency of 0.15±

Table 1 Structural chromosome aberrations in HeLa cells treated in G2 phase

Treatment	Cells scored	Abnormal cells (%)	Chromatid breaks (%)	Chromatid exchanges (%)	Complex exchanges (%)
Control	300	13 (4.3)	13 (4.3)	0	0
DMSO 0.5 %	300	14 (4.7)	14 (5.0)	0	0
NU7026 10 μM	300	24 (8.0)	24 (8.3)	0	0
ETO 2 μg/ml	300	228 (76.0)	689 (230.0)	227 (75.6)	21 (7.0)
NU7026-ETO	200	197 (98.5)*	963 (481.5)	290 (145.0)	12 (6.0)

*$p=0.0001$, chi-square test, ETO vs. NU7026-ETO

0.03 SCE per chromosome (NU7026=0.12 ± 0.05, $p=0.008$), which is a minor percentage of the DSB being repaired by HR in relation to ETO-treated cells. Therefore, in the presence of the DNA-PKcs inhibitor, the Rad51 foci formation in ETO-treated cells was associated with a less pronounced induction of SCE, indicating that the resolution of the HR events was affected.

ETO-induced DNA DSB progresses in post-mitotic G1 BN cells

To assess the role of DNA-PKcs in the progression of chromosomal damage, the occurrence of micronuclei in BN cells and the presence of γH2AX foci in micronuclei and in the main nuclei were evaluated in post-mitotic G1 phase cells (Fig. 3). Micronuclei are formed from an entire chromosome (aneugenic effect, γH2AX-negative micronuclei) or from a chromosome fragment (clastogenic effect, γH2AX-positive micronuclei) that lags behind at the anaphase of dividing cells and is not included in the main nucleus during telophase. As shown in Fig. 3a, following NU7026-ETO treatment, the percentage of BN cells with γH2AX signals in micronuclei increased ~3-fold compared with ETO. On the other hand, the proportion of BN cells without γH2AX foci in the micronuclei was similar in both treatments. Figure 3b shows the percentage of BN cells in different categories based on different γH2AX foci number in the main nuclei. This evaluation revealed that 69.7 ± 9.5 and 57.3 ± 7.6 % of the main nuclei did not contain γH2AX foci following ETO and NU7026-ETO treatments, respectively. An increase in the percentage of BN cells with γH2AX foci in nuclei was observed in both treatments, mainly in the group of 1–20 γH2AX foci. In addition, the combined NU7026-ETO treatment significantly diminished (~50 %) the percentage of BN cells, relative to ETO treatment alone (5.6 ± 1.6 vs. 10.5 ± 0.7 %) (Fig. 3c), as a consequence of

a higher accumulation of cells in G2/M phase at 10 h post-treatment (Supplementary Fig. S2). Taken together, the chemical inactivation of DNA-PKcs led to genome instability characterized by persistent DSB in the subsequent interphase BN cells.

MRE11 and DNA DSB foci correlate in ETO-treated BN cells when DNA-PKcs is inhibited

MRN complex, composed by MRE11, Rad50, and NBS1, acts as sensor of DNA damage and activates the DNA damage response-transducing kinase ATM. In addition, MRN participates in DSB end resection in G1 cells with a reduced role in comparison to G2-arrested cells, suggesting that initiation of break resection is less efficient in G1 cells (Symington and Gautier 2011).

To investigate whether MRE11 protein may be recruited to DSB in post-mitotic DNA-damaged cells, MRE11 and γH2AX co-localization was analyzed. We evaluated the presence of MRE11 foci in BN cells with γH2AX signals in the main nuclei at 10 h post-treatments. γH2AX foci were the result of persistent un-repaired or misrepaired events or recent DNA lesions generated during the previous mitosis. The degree of co-localization between these proteins was calculated by measuring coefficients M1 and M2 (Fig. 4; "Materials and methods"). The fraction of γH2AX signals associated with MRE11, M1 (Fig. 4a), and the fraction of MRE11 related to γH2AX signals, M2 (Fig. 4b), indicated that MRE11 signals co-localized with DNA DSB in response to both ETO and NU7026-ETO treatments; this conclusion was supported by the Pearson's correlation coefficient (Table 2). Notably, MRE11 and γH2AX showed the strongest correlation when a combined treatment was used ($r=0.584$, $p=0.005$) (Fig. 4c). From this study, it was evident that in G1
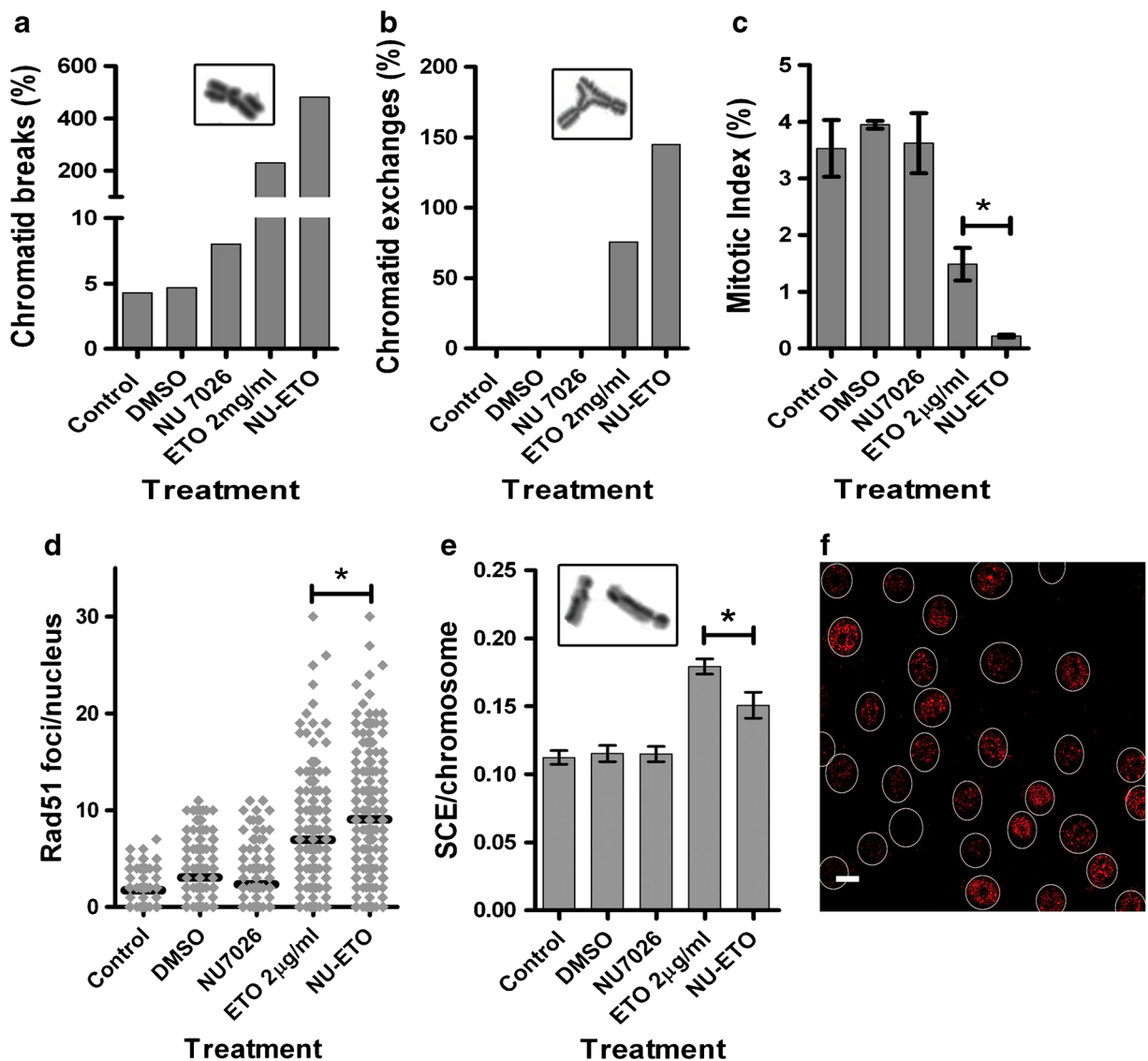
Fig. 2 Chromosomal damage and mitotic index induced by the different treatments in G2 HeLa human cells. Percentage of chromatid breaks (**a**), chromatid exchanges (**b**), and mitotic index (**c**) analyzed at the first metaphase post-treatment. *$p = 0.0001$, Student's t test. *Error bars* represent the SD from three to four independent experiments. Homologous recombination repair of DNA DSB induced by the different treatments in G2 HeLa human cells. **d** Rad51 foci formation. **e** Sister chromatid exchanges (*SCE*). *$p < 0.05$, Student's t test. *Error bars* reflect the SD of two or three independent experiments. **f** Representative image of HeLa nuclei with Rad51 foci after treatment with NU7026-ETO. *Insets* show representative examples of the structures scored. *Scale bar*, 15 μm

phase, there is an association between unresolved DSB and MRE11, mainly when DNA-PKcs is inhibited, demonstrating the contribution of MRE11 in the DSB repair by B-NHEJ.

In this sense, our preliminary data in HR-deficient cells treated with NU7062-ETO showed a pronounced accumulation of γH2AX foci in post-mitotic G1 BN cells, supporting a role of B-NHEJ in the repair of ETO-induced DNA damage (Supplementary Fig. S4).

DNA-PKcs inhibition and genome rearrangements in ETO-treated cells

The remaining DNA damage, observed 28 h after treatment, can lead to chromosome rearrangements in surviving cells. To identify the second metaphases following treatment, BrdU was incorporated for 8 h prior to preparation of chromosome spreads. In these metaphases, two types of rearrangements were considered:
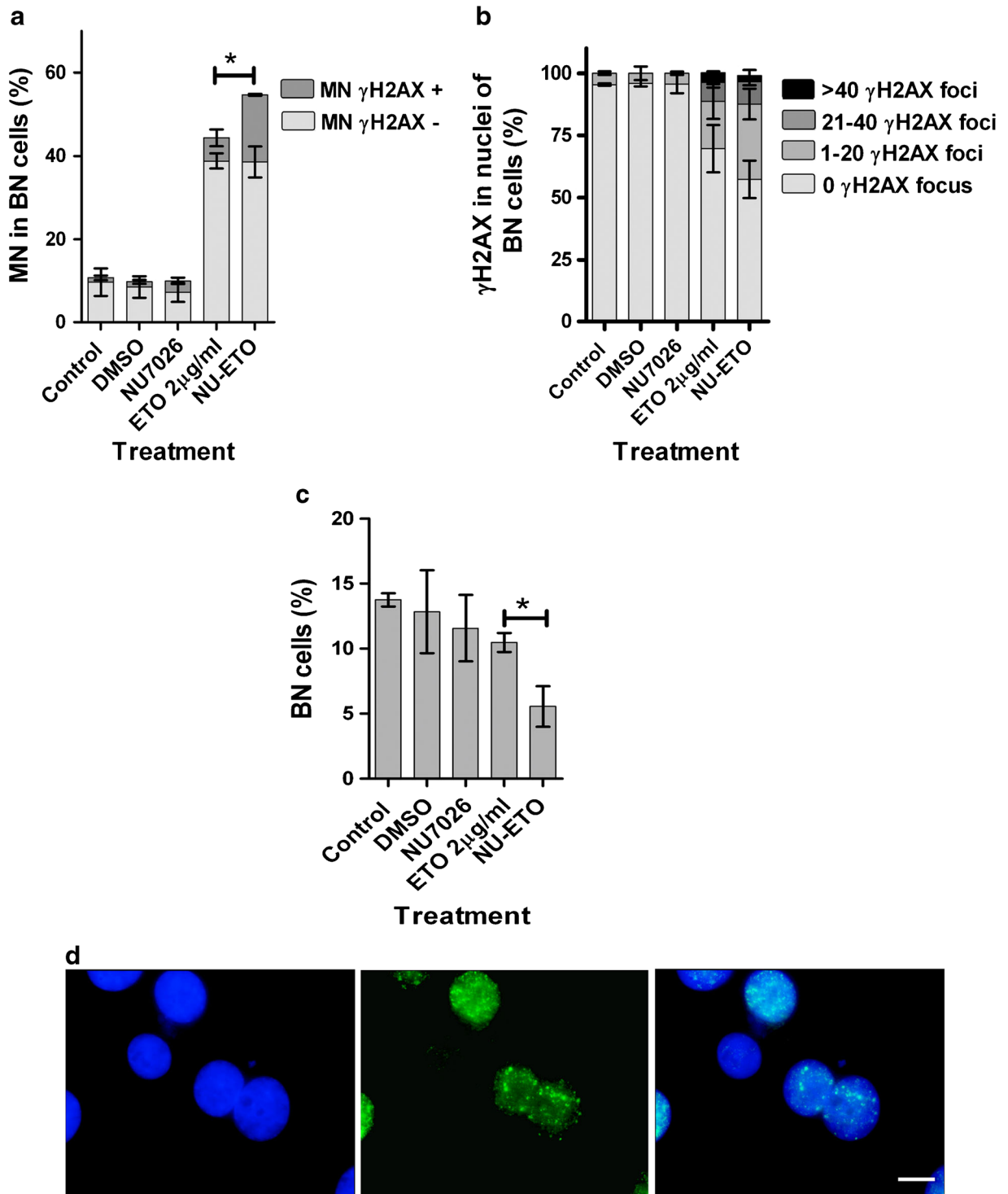
Fig. 3 Progression of DNA DSB (γH2AX foci) induced by the different treatments in G2 HeLa human cells and analyzed in post-mitotic G1 binucleated (*BN*) cells. **a** Percentage of micronucleated (*MN*) BN cells with or without γH2AX foci. *p=0.002, Student's t test between MN with γH2AX foci induced by ETO vs. those induced by NU7026-ETO. **b** Distribution of γH2AX foci number in the main nuclei of BN cells. **c** Percentage of BN cells. *p= 0.001, Student's t test. *Error bars* reflect the SD from three to four independent experiments. **d** Representative images of HeLa BN cells with γH2AX foci (FITC) in the main nuclei following ETO treatment for 1 h. DNA was stained with DAPI. *Scale bar*, 10 μm
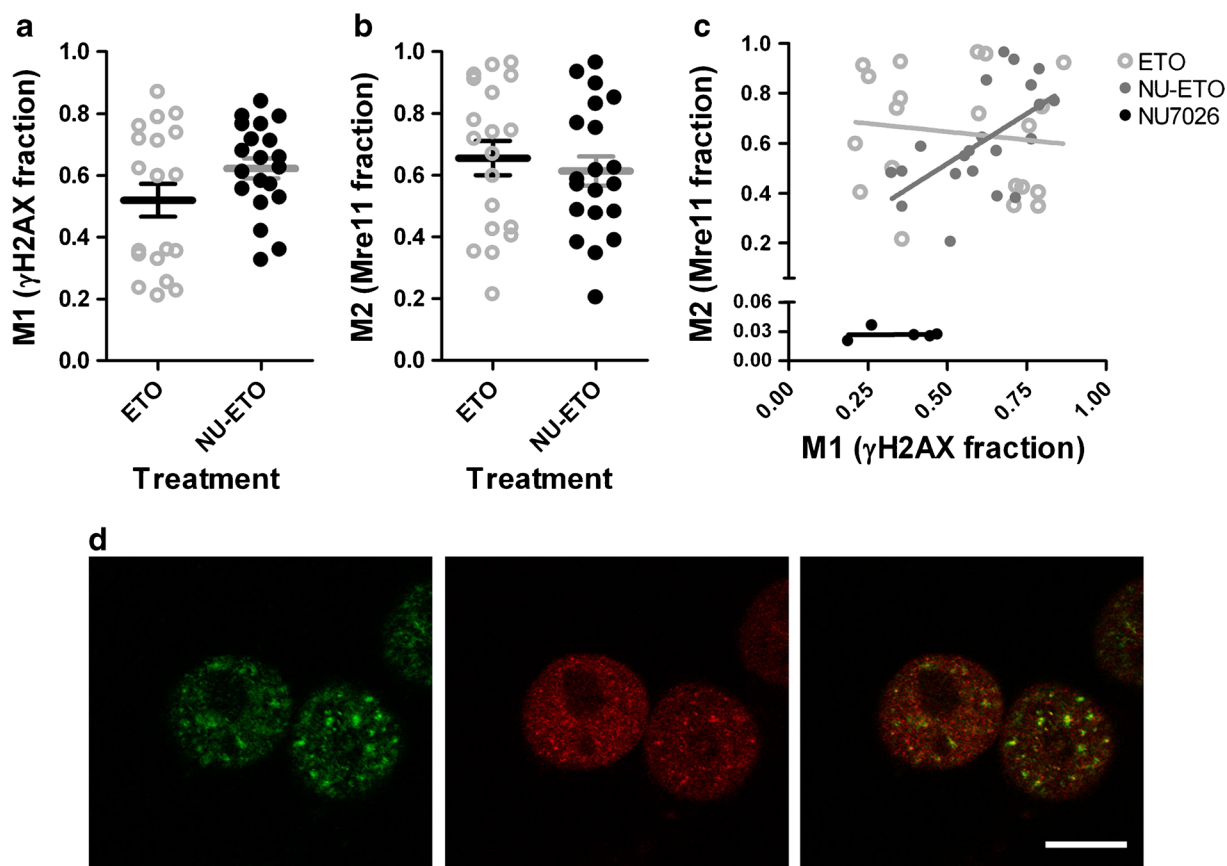
Fig. 4 DNA DSB (γH2AX) and MRE11 immunofluorescence analysis following ETO and NU7026-ETO treatments in HeLa human cells evaluated in post-mitotic G1 BN cells. **a** Fraction of γH2AX signals associated with MRE11, M1. **b** Fraction of MRE11 foci associated with γH2AX signals, M2. **c** Correlation relationships in response to ETO and NU7026-ETO treatments (control=NU7026). Three independent experiments were performed. **d** Representative deconvolved images of HeLa nuclei with γH2AX and MRE11 foci after treatment with NU7026-ETO. *Scale bar*, 10 μm

translocations and dicentric chromosomes; it has been established that in G2-irradiated cells, translocations and dicentrics are generated by identical mechanism (Yamauchi et al. 2011). First, we assessed the phosphorylation of H3 at serine 10 to identify mitotic cells. Results indicated that the combined treatment caused a decrease of ~26 % in the mitotic content, in contrast to ETO (Fig. 5a). When we evaluated the number of signals of chromosomes 1, 2, and 4 per cell by means of whole chromosome painting probes, data was similar for both treatments (ETO=9.4±1.2 and NU7026-ETO=

9.1±1.0) (Fig. 5b). On the other hand, as shown in Fig. 5c, following chemical inhibition of DNA-PKcs, the frequency of dicentric chromosomes was 1.4-fold increase after ETO treatment compared to ETO alone. Also, the percentage of cells with dicentric chromosomes was 33.3 and 26.2 % after NU7026-ETO and ETO treatments (NU7026-treated cells=12.0 %, p= 0.002), respectively. Hence, while the number of signals of chromosomes 1, 2, and 4 is similar irrespective of DNA-PKcs activity, its inhibition produced a slight increase in the number of dicentric chromosomes.

Table 2 Pearson's correlation coefficient (PCC)

Treatment	PCC (mean±SD)
ETO 2 μg/ml	0.669±0.118
NU7026-ETO	0.712±0.069

Discussion

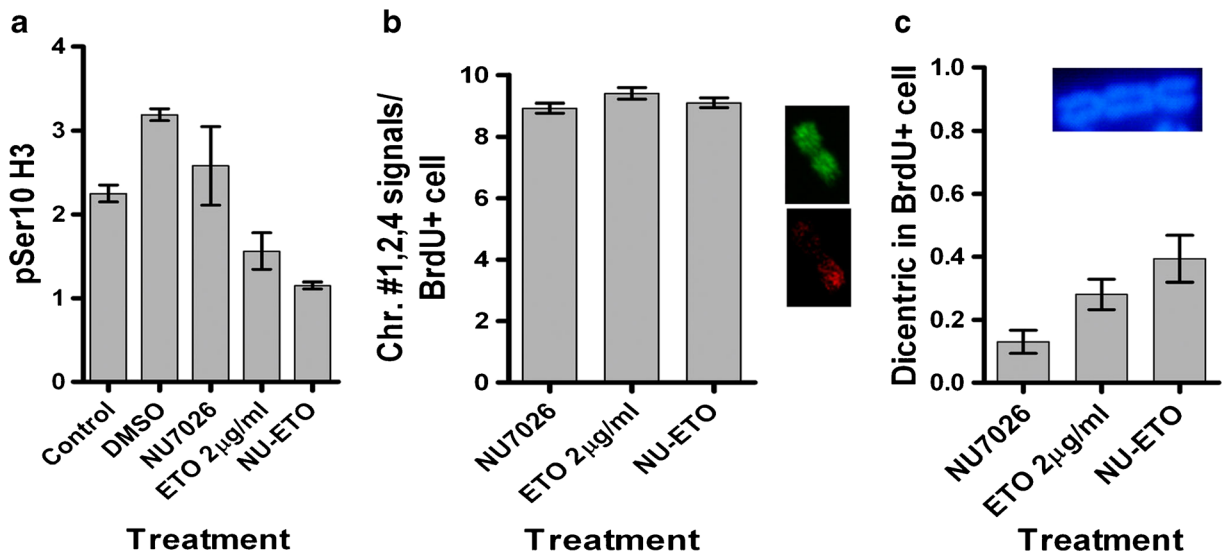Aberrant function of the DNA damage response leads to genomic instability, which could predispose cells to

Fig. 5 Chromosome rearrangements were evaluated in second metaphases of ETO- and NU7026-ETO-treated surviving HeLa cells. **a** Cells were immunostained with anti-phospho Ser10 histone H3 (indicator of mitosis) at 28 h post-treatments. *Error bars* reflect the SD of three independent experiments. **b** Whole chromosome painting-FISH signals probing chromosome nos. 1, 2, and 4 were scored in BrdU-positive cells. *Error bars* reflect the SD of two independent experiments. **c** Dicentric chromosomes were examined in BrdU-positive cells. *Error bars* reflect the SE of two independent experiments. *Insets* show representative examples of the structures scored

further mutations and increased risk of malignant transformation. The chemotherapy agent ETO is associated with therapy-related secondary leukemia in the treated patients. This drug induced an important increase of DSB in G2 enriched HeLa cells. Our previous data in normal human fibroblasts demonstrated that ETO increased DSB in all phases of the cell cycle and that D-NHEJ and HR pathways are involved in the repair of these lesions (de Campos-Nebel et al. 2010). Consistent with these results, Shibata et al. (2011) found that human fibroblasts rapidly repaired ETO-induced DSB in G2 by NHEJ, with only a small fraction being slowly repaired by HR. In addition to D-NHEJ and HR, recent studies demonstrated the function of a mechanism of DSB repair, which provides an alternative form of NHEJ (Dueva and Iliakis 2013).

DSB are the crucial lesions underlying the formation of chromosome aberrations (Obe and Durante 2010). Whereas an unrepaired DSB appears as a break at mitosis, misrepaired DSB generates intra- or inter-chromosomal exchanges. To evaluate the impact of DNA-PKcs in the DSB repair induced by ETO, we used the DNA-PKcs inhibitor NU7026. This inhibition increased the percentage of chromatid breaks and exchanges in HeLa cells treated in G2 in comparison to cells exposed to ETO alone. Since B-NHEJ is slower than D-NHEJ, DNA free

ends will have more time to move away from their original sites and eventually meet inappropriate ends for illegitimate reunion (exchange) or simply remain isolated and unrejoined (Durante et al. 2013). At 5–6 h post-treatment, ETO-induced accumulation of cells in G2 was increased by co-treatment with NU7026. In addition, the combined treatment correlated with a decline in cells subsequently entering mitosis, consistent with NU7026 potentiating the cytotoxicity of Top2 poisons (Willmore et al. 2004).

Subsequently, we evaluated whether the impairment of DNA-PKcs affects HR activity. In the presence of NU7026, ETO induced an increase of Rad51 foci formation, which was accompanied by a reduction of SCE compared to ETO-treated cells. The effect of DNA-PKcs deficiency on HR remains controversial. Several reports employing chemical and genetic approaches showed that the induction (Allen et al. 2002; Shrivastav et al. 2009; Neal et al. 2011) or repression (Allen et al. 2003; Convery et al. 2005) of DSB-induced HR repair was regulated by DNA-PKcs. Moreover, results from Bee et al. (2013) suggested that the recruitment of Rad51 at DSB sites in either NU7026-treated or DNA-PKcs-deficient human cells was delayed and persisted in relation to DNA-PKcs-proficient cells.

In relation to these observations, our results suggest that chemical inhibition of DNA-PKcs impaired both D-NHEJ and HR repair pathways, altering the maintenance of chromosomal integrity and the normal proliferative capacity after treatment in G2 with the Top2 poison ETO.

To determine the influence of this deficiency on the outcome of ETO-induced DSB, we examined the occurrence of γH2AX signals in MN and in main nuclei of post-mitotic binucleated cells. ETO promotes either structural or numerical chromosome aberrations originating in micronuclei with γH2AX-positive or γH2AX-negative signals, respectively. The combination with NU7026 caused an important increase in micronuclei with γH2AX-positive signals, without modifying the proportion of γH2AX-negative micronuclei in G2-treated HeLa cells. The formation of micronuclei was associated with the chromosome instability phenotype, which is often seen in cancer development (Fenech 2006). Likewise, the incidence of γH2AX foci in the main nuclei may reflect persistent DSB that were unrepaired and/or misrepaired or, alternatively, recent DSB that were formed via breakage of anaphase bridges originated by exchange-type aberrations in the subsequent G1. DNA-PKcs chemical inhibition resulted in a slight increase of ETO-induced damage in the next cell cycle.

We also investigated the contribution of MRE11 to the ETO-induced DSB repair after the chemical depletion of DNA-PKcs. MRE11 is recruited to DSB for their subsequent resolution, i.e., resecting and tethering DNA ends. In S/G2 phases, when sister chromatids are available, the nuclease activity of MRE11 contributes to DSB end resection to generate single-stranded DNA during HR repair (Shibata et al. 2014). Consequently, this mechanism could not operate in G1. Previous reports have established the involvement of MRN complex in the NHEJ repair of ETO-induced DSB in G1 (Robison et al. 2007; Quennet et al. 2011). Moreover, the participation of MRE11 in C- and in A-NHEJ by studying the repair of I-SceI endonuclease-induced DSB in mammalian cells has been established (Rass et al. 2009; Xie et al. 2009). Whereas MRE11 can favor A-NHEJ by initiating single-stranded DNA end resection, during C-NHEJ, it may promote tethering of the two ends of DSB, which facilitates its correct joining.

Our results indicate a close association between γH2AX and MRE11 foci in post-mitotic binucleated cells following ETO and NU7026-ETO treatments and a positive statistical correlation involving both proteins

in the combined treatment. This suggests that unresolved DSB have undergone end resection as evidenced by MRE11 loading. Thus, the stimulation of DNA end resection in G1 phase appears to be a critical factor in promoting tumorigenic chromosomal rearrangements (Symington and Gautier 2011). Based on this, we tested the presence of translocations and dicentric chromosomes in the second metaphase, 28 h following treatment. The analysis of these exchange-type chromosome aberrations is compatible with a G1 checkpoint defect that allows cells with persistent DSB to go through the cell cycle. It has been established that HeLa cells express defects in p53 signaling (Del Nagro et al. 2014), and we have confirmed, by flow cytometry, a lack of G1 arrest in asynchronously growing cells treated with increasing doses of ETO (data not shown).

We used FISH analysis to monitor translocations involving chromosomes 1, 2, and 4. ETO in combination with the DNA-PKcs inhibitor did not change the number of these chromosome signals when compared to NU7026- or ETO-treated cells. Results obtained in relation to chromosome translocation induction by C- or A-NHEJ were not conclusive in mammalian cells. It was demonstrated that A-NHEJ is the primary mediator of translocation formation in the absence of the C-NHEJ components, XRCC4/Lig IV (Simsek and Jasin 2010; Soni et al. 2014). In contrast, Ghezraoui et al. (2014) reported that translocation formation was generated by C-NHEJ as indicated by its reduction in the absence of Lig IV 4 or XRCC4.

In order to evaluate rearrangements on the whole genome level, we scored dicentric events and found that in the presence of NU7026, ETO caused a small increase in this frequency. This result agrees with a previous study of Yamauchi et al. (2011), which indicates that DNA-PKcs has some role in suppressing the occurrence of dicentric chromosomes following gamma irradiation in normal human fibroblasts.

Finally, with respect to time course analysis of HeLa cells treated in G2 phase with NU7026-ETO, we observed an important reduction of mitotic cells at 5–6 h post-treatment. However, at 10–11 h, cells released from G2/M entered the post-mitotic G1 phase with an increased number of binucleated cells. At 28 h post-treatment, the decrease of mitosis was less pronounced in comparison to cells only treated with ETO. Consequently, it was observed that HeLa cells slowly recovered into proliferation as the time following drug treatment increased.

In conclusion, we propose that ETO treatment in G2 cells, which are deficient for active DNA-PKcs, results in unfavorable genetic end points, such as micronuclei and dicentric chromosomes, which drive genome instability during cell progression. In this sense, Gascoigne and Cheeseman (2013) have reported that the induction of a single dicentric chromosome can contribute to genomic rearrangements and promote cellular transformation and tumorigenesis. Thus, the development and appearance of malignant clones that are responsible for therapy-related tumors may depend on the chemosensitizing effectiveness of the DNA-PKcs inhibitor versus the potential survival of aberrant cells with unrepaired or misrepaired DNA lesions.

Conflict of interest   The authors declare that they have no competing interests.

References

Allen C, Kurimasa A, Brenneman MA et al (2002) DNA-dependent protein kinase suppresses double-strand break-induced and spontaneous homologous recombination. Proc Natl Acad Sci U S A 99:3758–3763

Allen C, Halbrook J, Nickoloff JA (2003) Interactive competition between homologous recombination and non-homologous end joining. Mol Cancer Res 1:913–920

Bee L, Fabris S, Cherubini R et al (2013) The efficiency of homologous recombination and non-homologous end joining systems in repairing double-strand breaks during cell cycle progression. PLoS One 8:e69061

Boboila C, Oksenych V, Gostissa M et al (2012) Robust chromosomal DNA repair via alternative end-joining in the absence of X-ray repair cross-complementing protein 1 (XRCC1). Proc Natl Acad Sci U S A 109:2473–2478

Convery E, Shin EK, Ding Q et al (2005) Inhibition of homologous recombination by variants of the catalytic subunit of the DNA-dependent protein kinase (DNA-PKcs). Proc Natl Acad Sci U S A 102:1345–1350

Cowell IG, Austin CA (2012) Mechanism of generation of therapy related leukemia in response to anti-topoisomerase II agents. Int J Environ Res Public Health 9:2075–2091

Darroudi F, Natarajan AT (1989) Cytogenetical characterization of Chinese hamster ovary X-ray-sensitive mutant cells, xrs 5

and xrs 6. IV. Study of chromosomal aberrations and sister-chromatid exchanges by restriction endonucleases and inhibitors of DNA topoisomerase II. Mutat Res 212:137–148

de Campos-Nebel M, Larripa I, González-Cid M (2010) Topoisomerase II-mediated DNA damage is differently repaired during the cell cycle by non-homologous end joining and homologous recombination. PLoS One 5:e12541

Del Nagro CJ, Choi J, Xiao Y et al (2014) Chk1 inhibition in p53-deficient cell lines drives rapid chromosome fragmentation followed by caspase-independent cell death. Cell Cycle 13:303–314

Deweese JE, Osheroff N (2009) The DNA cleavage reaction of topoisomerase II: wolf in sheep's clothing. Nucleic Acids Res 37:738–748

Dueva R, Iliakis G (2013) Alternative pathways of non-homologous end joining (NHEJ) in genomic instability and cancer. Transl Cancer Res 2:163–177

Durante M, Bedford JS, Chen DJ et al (2013) From DNA damage to chromosome aberrations: joining the break. Mutat Res 756:5–13

Elguero ME, de Campos-Nebel M, González-Cid M (2012) DNA-PKcs-dependent NHEJ pathway supports the progression of topoisomerase II poison-induced chromosome aberrant cells. Environ Mol Mutagen 53:608–18

Fenech M (2006) Cytokinesis-block micronucleus assay evolves into a "cytome" assay of chromosomal instability, mitotic dysfunction and cell death. Review. Mutat Res 600:58–66

Gascoigne KE, Cheeseman IM (2013) Induced dicentric chromosome formation promotes genomic rearrangements and tumorigenesis. Chromosom 21:407–418

Ghezraoui H, Piganeau M, Renouf B et al (2014) Chromosomal translocations in human cells are generated by canonical non homologous end-joining. Mol Cell 55:829–842

Hsu FM, Zhang S, Chen BP (2012) Role of DNA-dependent protein kinase catalytic subunit in cancer development and treatment. Transl Cancer Res 1:22–34

Jeggo PA, Caldecott K, Pidsley S et al (1989) Sensitivity of Chinese hamster ovary mutants defective in DNA double strand break repair to topoisomerase II inhibitors. Cancer Res 49:7057–7063

Jin S, Inoue S, Weaver DT (1998) Differential etoposide sensitivity of cells deficient in the Ku and DNA-PKcs components of the DNA-dependent protein kinase. Carcinogenesis 19:965–971

Kao GD, McKenna WG, Yen TJ (2001) Detection of repair activity during the DNA damage-induced G2 delay in human cancer cells. Oncogene 20:3486–3496

Katsube T, Mori M, Tsuji H et al (2011) Differences in sensitivity to DNA-damaging agents between XRCC4- and Artemis-deficient human cells. J Radiat Res 52:415–424

Leone G, Fianchi L, Pagano L et al (2010) Incidence and susceptibility to therapy-related myeloid neoplasms. Chem Biol Interact 184:39–45

Liao H, Winkfein RJ, Mack G et al (1995) CENP-F is a protein of the nuclear matrix that assembles onto kinetochores at late G2 and is rapidly degraded after mitosis. J Cell Biol 130:507–518

Lieber MR (2010) The mechanism of double-strand DNA break repair by the nonhomologous DNA end-joining pathway. Review. Annu Rev Biochem 79:181–211

Manders EMM, Verbeek FJ, Aten JA (1993) Measurement of co-localization of objects in dual-colour confocal images. J Microsc 169:375–382

Mladenov E, Iliakis G (2011) Induction and repair of DNA double strand breaks: the increasing spectrum of non-homologous end joining pathways. Mutat Res 711:61–72

Mladenov E, Magin S, Soni A et al (2013) DNA double-strand break repair as determinant of cellular radiosensitivity to killing and target in radiation therapy. Front Oncol 3:113

Montecucco A, Biamonti G (2007) Cellular response to etoposide treatment. Cancer Lett 252:9–18

Morrison C, Vagnarelli P, Sonoda E et al (2003) Sister chromatid cohesion and genome stability in vertebrate cells. Biochem Soc Trans 31:263–265

Neal JA, Dang V, Douglas P et al (2011) Inhibition of homologous recombination by DNA-dependent protein kinase requires kinase activity, is titratable, and is modulated by autophosphorylation. Mol Cell Biol 31:1719–1733

Nitiss JL (2009) Targeting DNA topoisomerase II in cancer chemotherapy. Nat Rev Cancer 9:338–350

Obe G, Durante M (2010) DNA double strand breaks and chromosomal aberrations. Cytogenet Genome Res 128:8–16

Pendleton M, Lindsey RH Jr, Felix CA et al (2014) Topoisomerase II and leukemia. Ann N Y Acad Sci 1310:98–110

Quennet V, Beucher A, Barton O et al (2011) CtIP and MRN promote non-homologous end-joining of etoposide-induced DNA double-strand breaks in G1. Nucleic Acids Res 39:2144–2152

Rass E, Grabarz A, Plo I et al (2009) Role of Mre11 in chromosomal nonhomologous end joining in mammalian cells. Nat Struct Mol Biol 16:819–824

Robison JG, Dixon K, Bissler JJ (2007) Cell cycle-and proteasome-dependent formation of etoposide-induced replication protein A (RPA) or Mre11/Rad50/Nbs1 (MRN) complex repair foci. Cell Cycle 6:2399–2407

Sallmyr A, Tomkinson AE, Rassool FV (2008) Up-regulation of WRN and DNA ligase IIIα in chronic myeloid leukemia: consequences for the repair of DNA double-strand breaks. Blood 112:1413–1423

Shibata A, Conrad S, Birraux J et al (2011) Factors determining DNA double-strand break repair pathway choice in G2 phase. EMBO J 30:1079–92

Shibata A, Moiani D, Arvai AS et al (2014) DNA double-strand break repair pathway choice is directed by distinct MRE11 nuclease activities. Mol Cell 53:7–18

Shrivastav M, Miller CA, De Haro LP et al (2009) DNA-PKcs and ATM co-regulate DNA double-strand break repair. DNA Repair (Amst) 8:920–929

Simsek D, Jasin M (2010) Alternative end-joining is suppressed by the canonical NHEJ component Xrcc4-ligase IV during chromosomal translocation formation. Nat Struct Mol Biol 17:410–416

Soni A, Siemann M, Grabos M et al (2014) Requirement for Parp-1 and DNA ligases 1 or 3 but not of Xrcc1 in chromosomal translocation formation by backup end joining. Nucleic Acids Res 42:6380–6392

Symington LS, Gautier J (2011) Double-strand break end resection and repair pathway choice. Review. Annu Rev Genet 45:247–271

Tammaro M, Barr P, Ricci B et al (2013) Replication-dependent and transcription-dependent mechanisms of DNA double-strand break induction by the topoisomerase 2-targeting drug etoposide. PLoS One 8:e79202

Willmore E, de Caux S, Sunter NJ et al (2004) A novel DNA-dependent protein kinase inhibitor, NU7026, potentiates the cytotoxicity of topoisomerase II poisons used in the treatment of leukemia. Blood 103:4659–4665

Wu W, Wang M, Mussfeldt T et al (2008) Enhanced use of backup pathways of NHEJ in G2 in Chinese hamster mutant cells with defects in the classical pathway of NHEJ. Radiat Res 170:512–520

Xie A, Kwok A, Scully R (2009) Role of mammalian Mre11 in classical and alternative nonhomologous end joining. Nat Struct Mol Biol 16:814–818

Yamauchi M, Suzuki K, Oka Y et al (2011) Mode of ATM-dependent suppression of chromosome translocation. Biochem Biophys Res Commun 416:111–118